Nanoscale

Accepted Manuscript

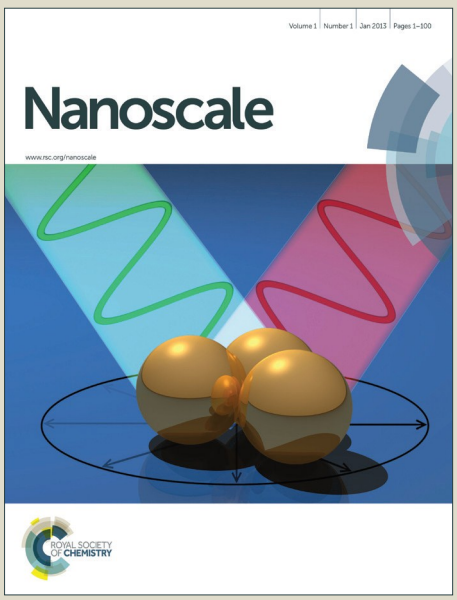

ROYAL SOCIETY OF CHEMISTRY

www.rsc.org/nanoscale

Chitin and Carbon Nanotube Composites as Biocompatible Scaffolds for Neuron Growth

Nandita Singh[1], Jinhu Chen[2], Krzysztof K Koziol[2], Keith R Hallam[3], Dawid Janas[2], Avinash J Patil[4], Ally Strachan[5], Jonathan Hanley[6] and Sameer S Rahatekar[7*]

1) School of Clinical Sciences, University of Bristol, Bristol BS2 8DZ, UK

2) Department of Materials Science and Metallurgy, University of Cambridge, Cambridge CB3 0FS, UK

3) Interface Analysis Centre, School of Physics, University of Bristol, Bristol BS8 1TL, UK

4) School of Chemistry, University of Bristol, Bristol BS8 1TS, UK

5) Centre for Nanoscience and Quantum Information, University of Bristol, Bristol BS8 1FD, UK

6) School of Medical Sciences, University of Bristol, Bristol BS8 1TD, UK

7) Advanced Composites Centre for Innovation and Science, Department of Aerospace Engineering, University of Bristol, Bristol BS8 1TR, UK

***Corresponding Author**

Dr Sameer S Rahatekar
Advanced Composites Centre for Innovation and Science
Department of Aerospace Engineering, University of Bristol, Bristol BS8 1TR, UK
Tel: +44 117331 5330
Email: sameer.rahatekar@bristol.ac.uk

Graphical Abstract

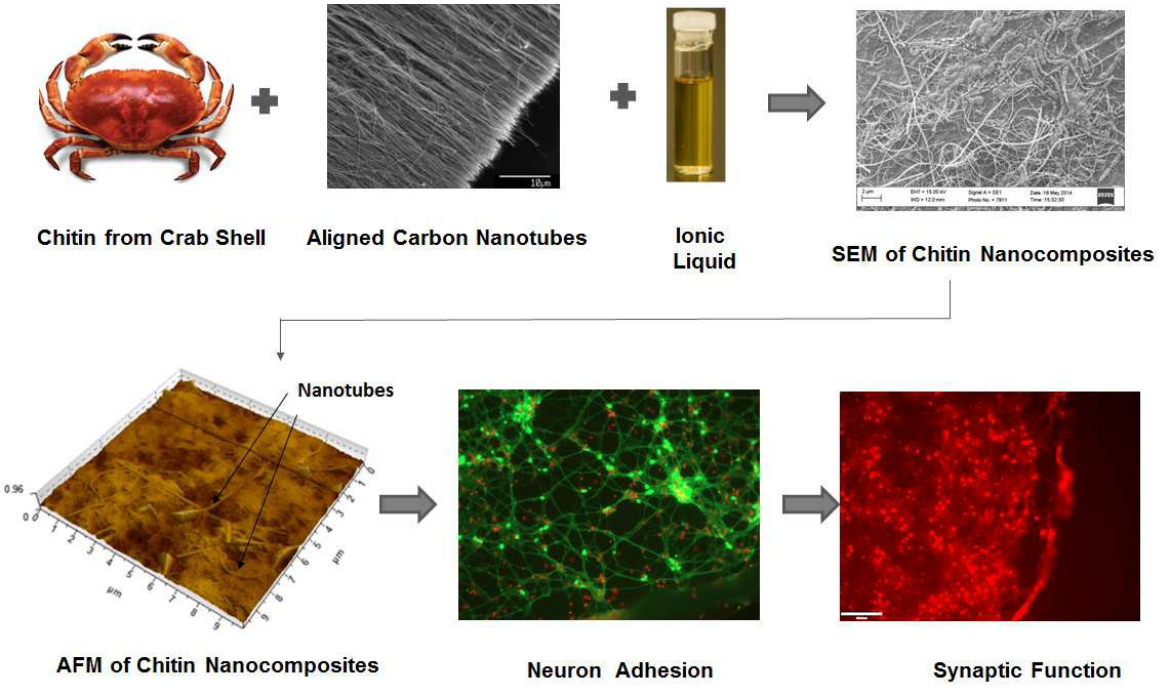

Abstract

Design of biocompatible implants for neurons repair/regeneration ideally requires high cell adhesion as well as good electrical conductivity. Here, we have shown that plasma-treated chitin carbon nanotube composite scaffolds show very good neuron adhesion as well as support of synaptic function of neurons. The addition of carbon nanotubes into chitin biopolymer improved the electrical conductivity and the assisted oxygen plasma treatment introduced more oxygen species onto the chitin nanotube scaffold surface. Neuron viability experiments showed excellent neuron attachment onto plasma-treated chitin nanotube composite scaffolds. The support of synaptic function was evident on chitin/nanotube composites, as confirmed by PSD-95 staining. The biocompatible and electrically-conducting chitin nanotube composite scaffold prepared in this study can be used for *in vitro* tissue engineering of neurons and, potentially, as an implantable electrode for stimulation and repair of neurons.

Keywords: Chitin, carbon nanotubes, ionic liquids, neurons, biomaterials.

1 Introduction

Nerve injuries can cause major trauma and even complete disability[1]. These injuries are not easily healed due to the complexity of the nervous system. Once the neurons in central nervous systems are damaged they are very difficult to repair [2]. Electrical stimulation has been shown to be most promising to enhance nerve regeneration [3-8] as well as stimulation of neural stem cells[9-11]. Hence, fabrication of electrically-conducting bioscaffolds capable of neural stimulation is an important area of study for neural tissue engineering. The electrically-conducting scaffolds need to be able to attract large number of neurons whilst being non-toxic. To design-in these multiple properties is, however, challenging. Here, we report on successfully growing neurons on electrically-conducting chitin/carbon nanotubes (CNTs) composites and show that these composites support and maintain synaptic function of neurons.

Chitin is not easy to dissolve in commonly used organic solvents. Hence, it was not widely used as a biomaterial for tissue engineering. However, recent developments in the ionic liquids based solvents allow effective dissolution and processing of chitin. It is now being used extensively in different forms, such as foams [12-14], fibres [15, 16], gels [17-19], micro particles [20], nanoparticles [21-23] and nanofibres [24-26], for a variety of biomedical applications [27-29]. Chitin is the second most abundant biopolymer after cellulose. Chitin and its derivatives have previously been shown to have a protective effect on neurons in early stage nerve injury [30, 31]. There is also evidence suggesting that chitin could negatively modulate Type 2 immune responses [32]. Accelerated nerve regeneration using induced pluripotent stem cells in chitin-chitosan-gelatine scaffolds with inverted colloidal crystal geometry has been observed [33]. 3D microporous scaffolds based on chitin alginate have been demonstrated to support efficient neuronal differentiation and maturation of human pluripotent stem cells[34].

Carbon nanotubes have been shown to have interesting material properties for neural interfaces in terms of electrochemical performance [35], as visualised with magnetic resonance and photo acoustic imaging. *In vivo* functionality of CNTs has also been demonstrated by successful registration of low-frequency neural recording in the live brain of anesthetised rats [36]. Pre-treating rats with amine-modified carbon nanotubes has been shown to protect neurons and enhance the recovery of behavioural functions in rats with induced stroke. Low levels of apoptotic, angiogenic and inflammation markers indicated that amine-modified carbon nanotubes protected the brains of treated rats from ischemic injury [37]. Hence, a bioscaffold prepared by combination of chitin and carbon nanotubes can potentially be very effective for neural tissue engineering.

To manufacture chitin/CNT composites we have used ionic liquids as a common platform for dissolution of chitin, as well as exfoliation/good dispersion of CNTs. In the present work, we have successfully grown neurons on electrically-conducting chitin/CNT composite films and have shown that these films, prepared using ionic liquid, can support the growth of neurons while maintaining their functional integrity. The stiffness of the chitin/CNT scaffolds prepared in this study (15-350 MPa) were higher than those of neurons or neural tissues[38] , however they were significantly lower than those of metal implants currently used for neural tissue engineering.

2 Materials and Methods

2.1 Preparation of the chitin nanotube films

Chitin (MW 100,000) was purchased from Heppe Medical Chitosan GmBH (Germany). The ionic liquid, 1-ethyl-3-methylimidazolium acetate (EMI Ac), was purchased from Sigma Aldrich and used as a solvent for chitin. All the tissue culture chemicals were purchased from Sigma, unless

otherwise stated. Two-dimensional chitin membranes were produced using the procedure described elsewhere [39]. Briefly, 1.5 % (mass fraction) of chitin was dissolved in 5 g of EMI Ac in a glass vial accompanied by constant heating and stirring for 2 h at 130 °C. After complete dissolution of chitin, multiwall carbon nanotubes (MWNTs) coated with carboxymethyl cellulose were used to prepare chitin and MWNT composite films. The coated MWNTs suspended in EMI Ac were then added to a chitin suspension to achieve 0.07 mass fraction of MWNTs with respect to the amount of chitin dissolved in EMI Ac. After the desired amount of MWNTs was suspended in chitin/EMI Ac solution, the solution was poured into a glass petri dish and allowed to cool for 3 h. The cooled solution was coagulated by adding ethanol to the petri dish. Ethanol selectively dissolves the EMI Ac and coagulates the chitin. The coagulated films were soaked in distilled water for 2 d to remove traces of EMI Ac and then dried at room temperature. Figure 1a shows a diagrammatic representation of the entire process for the preparation of membranes.

2.2 Plasma treatment

O_2 plasma treatment was carried out in a radio frequency plasma reactor (PlasmaPrep5, Germany). The plasma chamber was thoroughly purged with a continuous flow of the gas used during the treatment to reduce trace amounts of air and moisture. In total, four membranes were tested, i.e. neat chitin, chitin plasma-treated, chitin nanotubes untreated and chitin nanotubes plasma-treated. The test films were placed in a sterile petri plate and kept in the chamber. A power of 20 W was applied for 20 min on both sides of membranes. Neat chitin membrane was used as a control. All plasma treatments were carried out at room temperature.

2.3 Characterisation of chitin/CNTs composite films

2.3.1 Scanning electron microscopy (SEM): The cross-section and surface views of chitin and chitin/CNT films were analysed using SEM imaging with a field emission gun scanning electron microscope (JEOL JSM-6340 FEG-SEM) using an accelerating voltage of 15 kV and working distances between 15 mm and 6 mm. The SEM images were collect for untreated chitin, treated chitin, untreated chitin/CNTs and treated chitin/CNTs. At least two sets of each type of films were analysed using SEM. The films of chitin and chitin/CNTs composites were fixed to an aluminium stub with carbon pads. In order to avoid surface charging, a thin film of gold-palladium was sputtered for 15 s onto the samples with an EMITECH sputter coater.

2.3.2 Atomic force microscopy (AFM): AFM images were taken using either a Bruker (formerly Veeco) Dimension 3100 or Bruker Multimode IIIa. Images were taken in tapping mode in air using AppNano ATC-25 silicon cantilevers with a nominal tip radius of 10 nm and resonant frequency of 307 kHz. Drive amplitudes were often high to combat surface adhesion, but set points were kept at

80 % of free amplitude. 2 µm and 10 µm height and phase images, 512 px × 512 px in resolution, were collected. Nine horizontal lines were drawn on each image and average roughness was calculated using Gwydion software (version 2.38); data were further analysed using Graph Pad Prism version 5.03 software.

2.3.3 Electrical conductivity measurement: Measurement of electrical conductivity was carried out using a 2-point conductivity rig consisting of two copper electrodes separated by 2 mm distance. A precision LCR400 bridge (Thurlby Thandar Instruments, UK) was used to measure the resistance of the samples. In total, five samples were tested to get a good set of measurements. After measuring the resistance, the electrical conductivity was calculated as $\sigma = \frac{L}{R \cdot A}$, where *L* is the length of separation of the two electrical contact points/electrodes, *R* is the resistance and *A* is the cross-sectional area of the sample.

2.3.4 Hydrophilicity test: Dry membranes from all composites were cut with a biopsy punch to produce 8 mm diameter discs, which were attached with double-sided sticky tape to polyethylene substrate. 20 µl droplets of distilled water were placed onto the surface of the composites with a micropipette while images were recorded by a high-resolution camera (AVT Marlin F-131B), equipped with a macro lens, every three seconds onto the computer. Hydrophilicity measurement tests were carried out on at least three different parts of each type of film.

2.3.5 Nano indentation: Nano indentation tests were performed (MTS Nano Indenter XP) with a standard continuous stiffness measurement (CSM) method as follows: loading segment with a constant strain rate of 0.05 s^{-1} and a frequency of 45 Hz to a depth of 3 µm, a holding time of 10 s at the maximum applied force followed by unloading segment with the same rate of loading until 10 % of the maximum applied force is reached. A 4 µm Berkovich tip was used on all the measurements. The film samples were mounted on the aluminium stub. Proper calibrations on fused silica were performed immediately prior to the indentation tests on each type of sample. At least 10 measurements on different areas of each type of film were carried out. The average modulus measurements were reported at indentation depths between 2500 nm and 3000 nm.

2.3.6 X-ray photoelectron spectroscopy (XPS) analysis: A Thermo Fisher Scientific (East Grinstead, UK) Escascope spectrometer equipped with a dual anode X-ray source (Al Kα 1486.6 eV and Mg Kα 1253.6 eV) was used for XPS analysis. Samples were analysed under high vacuum (<5x10^{-8} mbar) with Al Kα radiation at 240 W (12 kV; 20 mA). Following the acquisition of survey spectra over a wide binding energy range, the C 1s, N 1s and O 1s spectral regions were then scanned at higher energy resolution such that valence state determinations could be made for each element. High resolution scans were acquired using 30 eV pass energy. Data analysis

was carried out using Pisces software (Dayta Systems, Bristol UK) with binding energy values of the recorded lines referenced to the adventitious hydrocarbon C 1s peak at 284.8 eV. The experiment was repeated on two sets of each type of membrane.

2.4 Cell culture

Dry membranes from all four composites were cut with a biopsy punch to produce 8 mm diameter discs. These were placed in a 24-well tissue culture plate. The membranes were disinfected with 0.7 volume fraction ethanol for 30 min and washed several times with sterile phosphate buffer saline (PBS). The membranes were coated with poly-L-lysine (100 µg/ml) overnight at 37 °C flowed by washing three times with PBS and were left to dry overnight in the incubator. Four hours before the cells were ready for loading, 200 µl of plating medium was added to the membranes and they were maintained at 37 °C and 5 % CO_2.

Dissociated cortical cultures were prepared from embryonic day 18 (E18) Wistar rats. All animals were handled in accordance with Home Office guidelines and University of Bristol standards. Following dissection and removal of meninges, cortices were isolated and rinsed three times in Hank's Balanced Salt Solution (HBSS, Gibco), then incubated in 18 ml HBSS containing Trypsin-EDTA at 37 °C for 15 min. Cells were washed a further three times in HBSS and then once in plating medium (Gibco Neurobasal medium containing 10 % horse serum (Gibco), 2 % B27 supplement (Gibco), 2 mM L-Glutamine (Gibco) and 1 % Penicillin/Streptomycin (Sigma)) and then mechanically triturated in 5 ml of plating medium to dissociate cells. The triturated cell suspension was then filtered through a 70 µm nylon mesh sterile cell strainer (Fisher Scientific) and the density of cells in suspension was determined using a haemocytometer.

Cells were plated on the poly-L-lysine treated scaffolds at a density of 2.5×10^5 cells per well and incubated at 37 °C with 5 % CO_2. After four hours of incubation, the plating medium was replaced with feeding medium (Gibco Neurobasal medium containing 2 % B27 supplement (Gibco) and 1 % Penicillin/Streptomycin (Sigma)) and cells were left to grow, with the addition of feeding medium every 5-6 days. Anti-mitotic agents FDU (Sigma F0503) and Uridine (Sigma U3003) were added with feeding medium (final concentration of 0.25 µM) after five days *in vitro* (DIV), to prevent proliferation of glia. Cells seeded on plastic as positive controls were maintained in the same medium.

2.5 Cell adhesion and viability assay

Live monitoring of cell adhesion and viability was conducted using the Live/Dead Viability/Cytotoxicity Kit for mammalian cells (Invitrogen, Paisley, UK), as per manufacturer's instructions.

Cell-loaded scaffolds were incubated for 7 d, 14 d and 21 d at 37 °C in a humidified atmosphere of 0.05 volume fraction CO_2 and 0.95 volume fraction air. The constructs were washed with PBS and incubated with calcein-AM, emission 488 nm (live cells) and ethidium homodimer-1, emission 568 nm (dead cells). Briefly, calcein-AM is membrane-permeable but, once inside the cell, the AM group is cleaved by cellular esterases trapping the calcein in the cell. A loss of cell membrane integrity allows the cleaved calcein to leak from the cell into the surrounding medium, leaving only the intact viable cells to fluoresce green. Dead cells, which retain ethidium homodimer-1 through damaged membranes, produce red fluorescence. Negative controls, consisting of cells killed with methanol, and positive controls, consisting of cells grown on plastic tissue culture plates, were run with each set of experiments. The plates were viewed under a digital fluorescence microscope system (Leica DMIRB inverted microscope, Houston, TX, USA). Experiments were repeated multiple times until a correct loading density was reached with not a huge population of cells, which could make the imaging difficult. The viability assay was repeated thrice in each case with four replicates of each scaffold.

2.6 Testing for synaptic strength

Postsynaptic density protein 95 (PSD-95) staining was carried out to test the presence of synaptic machinery of neurons growing on the composites. Neurons growing on all four composites were washed with PBS and fixed with 4 % ($^{w}/_{v}$) paraformaldehyde at room temperature after 21 d. The cells were permeabilised with 0.1 % ($^{v}/_{v}$) Triton X-100 in PBS containing 10 % (w/v) BSA at room temperature. The films were incubated with goat anti-mouse PSD-95 antibody (Abcam) overnight at 2 °C - 8 °C. The films were incubated with fluorescent secondary antibody (Northern Lights 557 Fluorochrome-conjugated donkey anti-goat secondary antibody; R&D Systems) and DAPI for 60 min at room temperature. The membranes were washed with PBS and images taken using a Leica wide-field fluorescence microscope. Negative controls included samples without the primary antibodies. The experiment was repeated twice with four replicates of each membrane.

2.7 Statistical analysis

One-way ANOVA with Turkey's multiple comparison post-hoc test was carried out and a significance level was set at 0.05. A mean +/- standard deviation format has been used to present the data for roughness analysis (Figure 3b). A minimum of four images were taken to analyse percentage fluorescent area using Image J. All the data obtained for fluorescent imaging were statistically evaluated using PRISM. Paired t-test analysis and two-way ANOVA were carried out and results with p value less than 0.05 were considered significant (Figure 7).

3 Results

3.1 Morphological changes of chitin/CNTs films by plasma treatment

SEM analysis was carried out to investigate the surface structure and morphology of films prepared from chitin/CNT composites after assisted O_2 plasma treatment. Figure 2 presents results of SEM of the films at low (Figures 2a, c, e and g) and high (Figures 2b, d, f and h) magnification. Cross-section and close-up surface views of untreated chitin film (Figure 2 a/b) show uniform dispersion and regeneration of chitin. Plasma treatment of chitin film (Figure 2 c/d) does seem to somewhat change the morphology of the film, with the surface becoming more irregular. Untreated chitin/CNTs film shows the irregular surface with the nanotubes still embedded inside the top layer of regenerated chitin (Figure 2 e/f). Plasma-treated chitin/CNTs film (Figure 2 g/h) however shows a rough surface morphology, with the surface being eroded by plasma treatment, leading to exposure of nanotubes on the surface. The interconnected network of carbon nanotubes is visible in the plasma-treated chitin/CNTs film, which can help to achieve electrical conductivity in this composite scaffold.

AFM imaging was used to determine fine changes in the topographic features. Figure 3a shows the topography and surface roughness of the prepared composites. Figure 3a(i) represents the surface topography of untreated chitin while Figure 3a(ii) show the granular topography present after plasma treatment of the same film. Chitin/CNTs film shows embedded nanotubes inside the film with a smooth top layer of chitin, as seen in Figure 3a(iii). Figure 3b shows the comparison of surface roughness for all scaffolds; the surface roughnesses were calculated using the method mentioned in Section 2.3.2. As seen in this figure, the plasma treatment process significantly increases the surface roughness of treated chitin compared to untreated chitin scaffolds. Similarly-treated chitin/CNTs scaffolds show significant increase in surface roughness as compared untreated chitin/CNTs scaffolds after plasma treatment.

Plasma-treated chitin/CNTs composite also revealed a rough surface with the presence of nanotubes on the surface (Figure 3a (iv)). Like SEM imaging previously, the interconnected nanotube network was also visible in the AFM images obtained.

3.2 Surface chemical modification by plasma treatment

Plasma treatment was shown to be a very effective method to increase adhesion of different cell types on various biomaterials[40,41]. Oxygen plasma treatment is commonly used to introduce hydrophilic surfaces onto fabricated polymers. These result in more oxygen-containing functional groups, which were obvious in the XPS analysis performed. Figure 4 and Table 1 show the atomic composition results from XPS analysis of all four scaffolds tested. Plasma-treated chitin and

plasma-treated chitin/CNTs composite showed decreases in the carbon composition after plasma treatment, with the untreated chitin having 67.8 % carbon composition, the plasma-treated chitin 63.1 %, untreated chitin/CNTs 63.9 % and plasma-treated chitin/CNTs composite scaffold 53.9 % carbon. While the composition of carbon was reduced after plasma treatment, the composition of oxygen went up significantly in plasma-treated chitin and plasma-treated chitin/CNTs composite scaffold, with increases from 22.5 % to 29.0 % for chitin to 40.5 % for chitin/CNTs composite. In addition, the ratio of surface oxidised carbon species to unoxidised carbon species was seen to rise from 1.3 to 1.7 for chitin and up to 4.3 for chitin/CNTs composite. The overall picture represents an increase in surface oxygen species for both chitin and chitin/CNTs after plasma treatment. This increased oxygen content can lead to increased hydrophilicity of the concerned surface.

3.3 Electrical conductivity of chitin/CNTs composite films

The electrical conductivity of untreated chitin/CNTs composite membrane was found to be 0.73 (±0.28) S/m. The electrical conductivity of plasma-treated chitin/CNTs scaffolds was found to be 2.89 (±0.54) S/m. Neat chitin and plasma-treated chitin were found to be non-conducting, as expected.

3.4 Hydrophilicity test using spreading of water droplet on scaffold surface

In order to study the change in hydrophilicity before and plasma treatment of the membranes, water droplet contact angle/contact time measurements were carried out. Figure 5a shows the series of images of spreading of water droplets over neat chitin, plasma-treated chitin, neat chitin/CNTs and plasma treat chitin/CNTs membranes at 3, 30 and 60 seconds. The neat chitin and plasma-treated chitin membranes show quick spreading of the droplet without any appreciable difference between these two membranes. However, the spread of the water droplet on the untreated chitin/CNTs membranes was seen to be significantly slower (even after 60 seconds) than neat chitin and plasma-treated chitin membranes. This is a strong indication that the untreated chitin/CNTs membrane is not likely to be very hydrophilic. The spread of the water droplet on plasma-treated chitin/CNTs was seen to be significantly higher than that of the untreated chitin/CNTs membrane. This again is a strong indication that the plasma-treated chitin/CNTs is more hydrophilic than the untreated chitin/CNTs membrane.

3.5 Nano indentation

The nano indentation tests were carried out as described in the Section 2.3.5. Figure 5b shows the moduli of untreated chitin, plasma-treated chitin, untreated chitin/CNTs and plasma-treated chitin/CNTs composite scaffolds. As seen in Figure 4b, the moduli range from 160 to 420 MPa for

the four scaffolds. The addition of carbon nanotubes seems to increase the moduli of the scaffolds.

3.6 Neuronal viability on the electrically-conducting, plasma-treated chitin/CNTs composites

Biocompatibility and the survival potential of neurons on all the four scaffolds were tested using the Live/Dead viability assay, as described in Section 2.5, where green fluorescence indicates live cells and red fluorescence shows dead cells. As seen in Figures 6.1a1 and 6.2a1, a large proportion of live cell attachment was observed after 7 d and 14 d on untreated chitin films. However, when chitin films were plasma-treated the cell attachment was enhanced (Figures 6.1b1 and 6.2b1). No cell adhesion was seen in untreated chitin/CNTs films after 7 d and the cells seemed to cluster together into small patches (Figures 6.1c1 and 6.2c2). A large number of dead cells were seen after 14 d on this membrane. These dead cells hardly showed any attachment and were seen floating in small patches in the petri dish. The plasma-treated chitin/CNTs scaffolds showed excellent viable adhesion of neurons after 7 d, which significantly increased further after 14 d (Figures 6.1d1 and 6.2d2, Figure 7). Images for positive controls using cells seeded on plastic (both live-green and dead-red) (Figures 6.1e1 and 6.2e1) and negative controls using cells killed by methanol (Figure 6.2e2) are shown for comparison. No dead cells were obtained on the positive control after 7 d; hence, no red signal was obtained. The total cell attachment after 14 d on treated chitin/CNTs membranes was significantly higher compared to the untreated chitin, chitin treated and untreated chitin/CNTs membranes (Figure 7).

3.7 PSD-95 expression in neurons on chitin/CNTs composites

PSD-95 is a major component of the post-synaptic density (PSD). The protein interacts with a wide variety of membrane and cytoplasmic proteins to form a large signalling complex, promotes the maturation and strengthening of excitatory synapses and is required for activity-driven synapse stabilisation. We, therefore, carried out PSD-95 immunocytochemistry to determine the presence of synapses on neurons growing on the four scaffolds. The cells were counter-stained by DAPI. Untreated chitin and plasma-treated chitin films showed good PSD-95 expression (Figures 8a2 and b2) as also did the plasma-treated chitin/CNTs (Figure 8.d2). However, untreated chitin/CNTs film again showed no cell attachment or unattached cells floating in small clumps (Figure 8c2, Figures 8a1, b1, c1 and d1 - nuclear staining for the neurons with DAPI - and Figures 8a3, b3, c3 and d3 - merged images of nuclear and PSD-95 marker). Figures 8e1 (nuclear staining) and e2 show positive control on plastic while Figures 8f1 (nuclear staining) and f2 show negative control, with no primary antibody. These data confirm that plasma-treated chitin/CNTs scaffolds were able to promote the appropriate expression of the synaptic protein machinery.

4 Discussion

With the incentive to reap the benefits of combining the biocompatible properties of chitin with the electrical conductive properties of nanotubes, chitin/CNTs films prepared using ionic liquids were subjected to neuron adhesion experiments. These composites were effectively shown to attach and sustain neurons and maintain their functional integrity after assisted O_2 plasma treatment, even after 21 d. Briefly, four different scaffolds were manufactured, namely neat chitin, plasma-treated chitin, untreated chitin/CNTs and plasma-treated chitin/CNTs scaffold.

Implantable scaffolds seem to be a promising path to treat brain injury. With currently no or only a limited number of drugs available to treat brain disorders, such as Alzheimer's and similar dementia diseases, the implantable scaffolds seem to be a promising option to promote regeneration of dying brain cells complete with their functional recovery. However, to design such a scaffold it is necessary to keep in mind that it should be electrically-conducting as well as soft and biocompatible, should minimise cell death and inflammation and support synaptic function in the long run. Hence, the choice of material becomes a crucial parameter. Natural polymer-based scaffolds can exhibit high bioactivity and maximum cell adhesion, but are difficult to surface engineer. On the other hand, MWNTs present rather attractive surfaces for their electrical properties but, according to Gladwin et al [42], for MWNTs to be used as scaffolds requires robust surface modification to enhance biocompatibility and cell adhesion. The study conducted in the current work showed excellent adhesion of neurons on O_2 plasma-treated chitin/CNTs scaffolds. XPS analysis confirmed an increase in oxygen species and decrease in carbon species, rendering the surfaces more hydrophilic. In addition, such surfaces had exposed nanotubes, rendering the surfaces even more rough and prone to promote neural synapsis[43]. We believe that the roughness in combination with increased oxygen content after plasma treatment led to better facilitation of neural adhesion and synaptic support. Variation in topography at the nanoscale level seems to modulate the behaviour of stem cells[44].

Measurement of surface roughness of the scaffolds revealed that plasma-treated chitin and plasma-treated chitin/CNTs composite scaffolds had significantly higher surface roughness than the untreated chitin and untreated chitin/CNTs (Figure 3b). On the other hand, viability assay and fluorescent image analysis (Figure 7) identified that the neuron adhesion was significantly higher after 14 d in plasma-treated chitin/CNTs scaffolds. This could be a combined effect of increased surface roughness and increased oxygen species compared to the remaining three types of scaffolds. Both these properties make the scaffold more bioactive and compatible for use as a suitable implant for regeneration of neurons. The change in the surface topography with has been shown to affect the cell adhesion, morphology, differentiation and survival[44].

Another reason for the dense binding of neurons on the three composites, namely untreated chitin, treated chitin and treated chitin/CNTs, is also supported by the fact the surface has become more hydrophilic as compared to untreated chitin/CNTs scaffolds. This is clearly evident by results from the hydrophilicity test experiment. The treated chitin/CNTs scaffold seems to possess a blend of the properties of treated chitin and untreated chitin/CNTs as initially the water droplet remains intact on the surface of the film, before it slowly gets absorbed.

However, with the addition of nanotubes in both the untreated chitin/CNTs and treated chitin/CNTs scaffolds we observe higher moduli compared to untreated and treated chitin (Figure 5b). The combined effect of the increased modulus and the hydrophobic nature makes the untreated chitin/CNTs scaffold unsuitable for cell adhesion. Plasma treatment of chitin/CNTs, on the other hand, makes the surface more hydrophilic with the increase in the ratio of oxygenated to unoxygenated carbon species from 1.6 to 4.3 (Figure 4 and Table 1), allowing cells to adhere.

The modulus of elasticity for the neurons has been reported to be between 3 and 6 kPa [45, 46]. The modulus of our membrane tested using nano indentation was found to be about 150 and 350 MPa. Even though this modulus of elasticity is much higher than that of neurons it is relatively less mismatch as compared to the metal electrodes (modulus well over 50,000 MPa) which are currently being used for regenerative therapy of neurons. The treated chitin/CNTs scaffold was surface modified by plasma treatment with increases in roughness, oxygen species and hydrophilicity.

Viability assays showed excellent adhesion of neurons in the plasma-treated chitin/CNTs after 7 d and 14 d. Previously, O_2 plasma-treated biomimetic nanofibrous scaffolds have been shown to enhance compatibility of cardiovascular implants [47]. Ion et al also demonstrated excellent adhesion and spreading of macrophage on plasma-treated carbon nanowalls [48]. This is consistent with what we observed in our current studies for adhesion of neurons on both plasma-treated chitin and chitin/CNTs composite scaffolds. The treated chitin/CNTs composite scaffolds showed a large degree of clustered growth of neurons. This suggests interaction of neurons with the plasma-treated chitin/CNTs is influenced not only by its chemical composition and mechanical properties but also by the nanoscale profile of the surface. This kind of behaviour was also observed by Wang et al [49], where the authors reported neurons bound and preferentially-anchored to rough, nano-engineered surfaces. Increased surface roughness, oxygen species and hydrophilicity seem to be major contributing factors for the cluster binding of neurons on these composites (Figures 6.2b1 and d1). Hence, despite the incorporation of nanotubes into a biological material, plasma treatment managed to render the surface rich-enough in oxygen

species for the cells to show significantly high cell attachment on plasma-treated chitin/CNTs film. (Figure 7).

It is important for a scaffold to also maintain surface functionality of the cell types in question. To confirm that the scaffolds not only promote neuronal survival but also support appropriate synaptic development, PSD-95 expression, which is a hallmark of excitatory synaptic function and plasticity, was studied on all four composites after 21 d. Results showed that plasma-treated chitin/CNT scaffolds exhibited strong PSD-95 staining. Untreated chitin (Figures 8a1, a2 and a3) also showed PSD-95 staining along with treated chitin (Figures 8b1, b2 and b3), revealing that chitin as a natural polymer also supports synaptic function but does not carry the advantage of being electrically-conducting. Since there was no cell attachment after 21 d on untreated chitin/CNTs, the membrane in itself was not found to be biologically significant (Figures 8c1, c2 and c3). Plasma-treated chitin/CNTs samples gave better signals (Figures 8d1, d2 and d3) and appeared equivalent to the control plastic tissue culture plate (Figures 8e1 and e2). Previously, nanotube-based scaffolds have been shown to be able to lead to increased connectivity by promoting synaptogenesis via modulation of deposition of an extracellular matrix more permissive for synapse construction [50]. Carbon nanotube platforms have also been shown to support network connectivity and synaptic plasticity in mammalian cortical circuits[43]. Carbon nanotube neuron hybrid networks have been shown to detect a boost in signal transmission with increase in frequency of synaptic events[51, 52]. Single-cell activity of an individual neuron has been shown to be affected when it interacts with a carbon nanotube substrate [53]. With all the supporting evidence, we can justify that the manufactured composites with the biopolymer and nanotube blend are still supportive to synaptic function and that nanotubes might play a role in synaptic transmission.

5 Conclusions

Using a combination of the biocompatible properties of chitin and the electrical conductivity of carbon nanotubes with assisted O_2 plasma treatment, we have developed a novel biocompatible and electrically-conducting scaffold for growth of neurons. Four types of scaffolds, namely neat chitin, plasma-treated chitin, untreated chitin/CNTs and plasma-treated chitin/CNTs, were manufactured using ionic liquids as solvents. Plasma treatment was used as a means for modification of surface topography as well as surface chemistry. Plasma treatment led to the alteration of surface topography, increased surface roughness, increased hydrophilicity and an increase in the amount of oxygen species present on the surface of the scaffolds. The plasma-treated chitin/CNTs composite scaffold showed increased neuron attachment compared to chitin scaffolds after 14 d. This effect was contributed to the increase in surface roughness as well as increased oxygen species content in the plasma-treated chitin/CNTs scaffold despite having

higher modulus compared to the other three scaffolds. Three scaffolds, namely neat chitin, plasma-treated chitin and plasma-treated chitin/CNTs, were found to support neural synapses (tested using PSD-95 staining), which suggests that the neurons are still functionally-active on these scaffolds after 21 d.

Acknowledgements

SSR would like to acknowledge partial funding from the University Research Committee, University of Bristol. NS would like to thank Zsombor Koszegi and Nick Carney, School of Biochemistry, University of Bristol for immense help in conducting the PSD-95 staining and viability experiments.

References

1. J. C. Rivera, G. P. Glebus and M. S. Cho, *The bone & joint journal*, 2014, **96-B**, 254-258.
2. M. V. Sofroniew and H. V. Vinters, *Acta neuropathologica*, 2010, **119**, 7-35.
3. A. Kotwal and C. E. Schmidt, *Biomaterials*, 2001, **22**, 1055-1064.
4. T. M. Brushart, P. N. Hoffman, R. M. Royall, B. B. Murinson, C. Witzel and T. Gordon, *The Journal of neuroscience : the official journal of the Society for Neuroscience*, 2002, **22**, 6631-6638.
5. A. A. Al-Majed, C. M. Neumann, T. M. Brushart and T. Gordon, *The Journal of neuroscience : the official journal of the Society for Neuroscience*, 2000, **20**, 2602-2608.
6. M. K. Gheith, T. C. Pappas, A. V. Liopo, V. A. Sinani, B. S. Shim, M. Motamedi, J. R. Wicksted and N. A. Kotov, *Adv Mater*, 2006, **18**, 2975-+.
7. M. P. Prabhakaran, L. Ghasemi-Mobarakeh, G. R. Jin and S. Ramakrishna, *J Biosci Bioeng*, 2011, **112**, 501-507.
8. J. T. Seil and T. J. Webster, *Wires Nanomed Nanobi*, 2010, **2**, 635-647.
9. J. Landers, J. T. Turner, G. Heden, A. L. Carlson, N. K. Bennett, P. V. Moghe and A. V. Neimark, *Adv Healthc Mater*, 2014, **3**, 1745-1752.
10. E. Jan and N. A. Kotov, *Nano letters*, 2007, **7**, 1123-1128.
11. N. W. S. Kam, E. Jan and N. A. Kotov, *Nano letters*, 2009, **9**, 273-278.
12. S. S. Silva, A. R. C. Duarte, A. P. Carvalho, J. F. Mano and R. L. Reis, *Acta Biomater*, 2011, **7**, 1166-1172.
13. Y. M. Zhou, S. Y. Fu, Y. Q. Pu, S. B. Pan and A. J. Ragauskas, *Carbohyd Polym*, 2014, **112**, 277-283.
14. K. S. Chow and E. Khor, *Biomacromolecules*, 2000, **1**, 61-67.
15. Y. Qin, X. M. Lu, N. Sun and R. D. Rogers, *Green Chem*, 2010, **12**, 968-971.
16. P. S. Barber, S. P. Kelley, C. S. Griggs, S. Wallace and R. D. Rogers, *Green Chem*, 2014, **16**, 1828-1836.
17. K. Prasad, M. Murakami, Y. Kaneko, A. Takada, Y. Nakamura and J. Kadokawa, *Int J Biol Macromol*, 2009, **45**, 221-225.
18. A. Takegawa, M. Murakami, Y. Kaneko and J. Kadokawa, *Carbohyd Polym*, 2010, **79**, 85-90.
19. Y. Wu, T. Sasaki, S. Irie and K. Sakurai, *Polymer*, 2008, **49**, 2321-2327.
20. S. S. Silva, A. R. C. Duarte, J. F. Mano and R. L. Reis, *Green Chem*, 2013, **15**, 3252-3258.
21. J. G. Torres-Rendon, F. H. Schacher, S. Ifuku and A. Walther, *Biomacromolecules*, 2014, **15**, 2709-2717.
22. J. D. Goodrich and W. T. Winter, *Biomacromolecules*, 2007, **8**, 252-257.
23. C. V. Nikiforidis and E. Scholten, *Rsc Adv*, 2015, **5**, 37789-37799.
24. P. S. Barber, C. S. Griggs, J. R. Bonner and R. D. Rogers, *Green Chem*, 2013, **15**, 601-607.
25. B. M. Min, S. W. Lee, J. N. Lim, Y. You, T. S. Lee, P. H. Kang and W. H. Park, *Polymer*, 2004, **45**, 7137-7142.
26. C. Zhong, A. Cooper, A. Kapetanovic, Z. H. Fang, M. Q. Zhang and M. Rolandi, *Soft Matter*, 2010, **6**, 5298-5301.
27. R. Jayakumar, M. Prabaharan, P. T. S. Kumar, S. V. Nair and H. Tamura, *Biotechnol Adv*, 2011, **29**, 322-337.
28. P. Mezzana, *Acta chirurgiae plasticae*, 2008, **50**, 81-84.
29. N. S. Rejinold, K. P. Chennazhi, H. Tamura, S. V. Nair and J. Rangasamy, *ACS applied materials & interfaces*, 2011, **3**, 3654-3665.
30. T. S. Vo, D. H. Ngo, Q. V. Ta, I. Wijesekara, C. S. Kong and S. K. Kim, *Cell Immunol*, 2012, **277**, 14-21.
31. A. S. a. P. Kothiyal, *Indo American Journal of Pharmaceutical Research*, 2014, **4**, 3689-3696.
32. C. G. Lee, *Yonsei Med J*, 2009, **50**, 22-30.
33. Y. C. Kuo and C. C. Lin, *Colloids and Surfaces B-Biointerfaces*, 2013, **103**, 595-600.
34. H. F. Lu, S. X. Lim, M. F. Leong, K. Narayanan, R. P. K. Toh, S. J. Gao and A. C. A. Wan, *Biomaterials*, 2012, **33**, 9179-9187.
35. E. B. Malarkey and V. Parpura, *Brain Edema Xiv*, 2010, **106**, 337-341.
36. H. Zhang, J. Shih, J. Zhu and N. A. Kotov, *Nano letters*, 2012, **12**, 3391-3398.
37. H. J. Lee, J. Park, O. J. Yoon, H. W. Kim, D. Y. Lee, D. H. Kim, W. B. Lee, N. E. Lee, J. V. Bonventre and S. S. Kim, *Nature Nanotechnology*, 2011, **6**, 120-124.
38. K. Franze, P. A. Janmey and J. Guck, *Annu Rev Biomed Eng*, 2013, **15**, 227-251.
39. N. Singh, K. K. K. Koziol, J. H. Chen, A. J. Patil, J. W. Gilman, P. C. Trulove, W. Kafienah and S. S. Rahatekar, *Green Chem*, 2013, **15**, 1192-1202.
40. S. Tunma, K. Inthanon, C. Chaiwong, J. Pumchusak, W. Wongkham and D. Boonyawan, *Cytotechnology*, 2013, **65**, 119-134.
41. S. De, R. Sharma, S. Trigwell, B. Laska, N. Ali, M. K. Mazumder and J. L. Mehta, *Journal of biomaterials science. Polymer edition*, 2005, **16**, 973-989.

42. K. M. Gladwin, R. L. D. Whitby, S. V. Mikhalovsky, P. Tomlins and J. Adu, *Adv Healthc Mater*, 2013, **2**, 728-735.
43. G. Cellot, F. M. Toma, Z. K. Varley, J. Laishram, A. Villari, M. Quintana, S. Cipollone, M. Prato and L. Ballerini, *Journal of Neuroscience*, 2011, **31**, 12945-12953.
44. P. Tsimbouri, N. Gadegaard, K. Burgess, K. White, P. Reynolds, P. Herzyk, R. Oreffo and M. J. Dalby, *Journal of cellular biochemistry*, 2014, **115**, 380-390.
45. E. Spedden, J. D. White, E. N. Naumova, D. L. Kaplan and C. Staii, *Biophys J*, 2012, **103**, 868-877.
46. Y. Q. Fang, C. Y. Y. Iu, C. N. P. Lui, Y. K. Zou, C. K. M. Fung, H. W. Li, N. Xi, K. K. L. Yung and K. W. C. Lai, *Sci Rep-Uk*, 2014, **4**.
47. A. M. Pappa, V. Karagkiozaki, S. Krol, S. Kassavetis, D. Konstantinou, C. Pitsalidis, L. Tzounis, N. Pliatsikas and S. Logothetidis, *Beilstein J Nanotechnol*, 2015, **6**, 254-262.
48. R. Ion, S. Vizireanu, C. E. Stancu, C. Luculescu, A. Cimpean and G. Dinescu, *Materials Science & Engineering C-Materials for Biological Applications*, 2015, **48**, 118-125.
49. W. Wang, S. Itoh, A. Matsuda, S. Ichinose, K. Shinomiya, Y. Hata and J. Tanaka, *J Biomed Mater Res A*, 2008, **84A**, 846-846.
50. N. Berardi, T. Pizzorusso and L. Maffei, *Neuron*, 2004, **44**, 905-908.
51. V. Lovat, D. Pantarotto, L. Lagostena, B. Cacciari, M. Grandolfo, M. Righi, G. Spalluto, M. Prato and L. Ballerini, *Nano letters*, 2005, **5**, 1107-1110.
52. A. Mazzatenta, M. Giugliano, S. Campidelli, L. Gambazzi, L. Businaro, H. Markram, M. Prato and L. Ballerini, *Journal of Neuroscience*, 2007, **27**, 6931-6936.
53. G. Cellot, E. Cilia, S. Cipollone, V. Rancic, A. Sucapane, S. Giordani, L. Gambazzi, H. Markram, M. Grandolfo, D. Scaini, F. Gelain, L. Casalis, M. Prato, M. Giugliano and L. Ballerini, *Nature Nanotechnology*, 2009, **4**, 126-133.

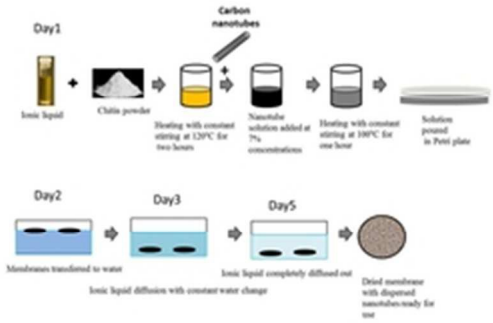

Figure1a. Schematic representation for the preparation of chitin/CNTs composite films.
30x17mm (300 x 300 DPI)

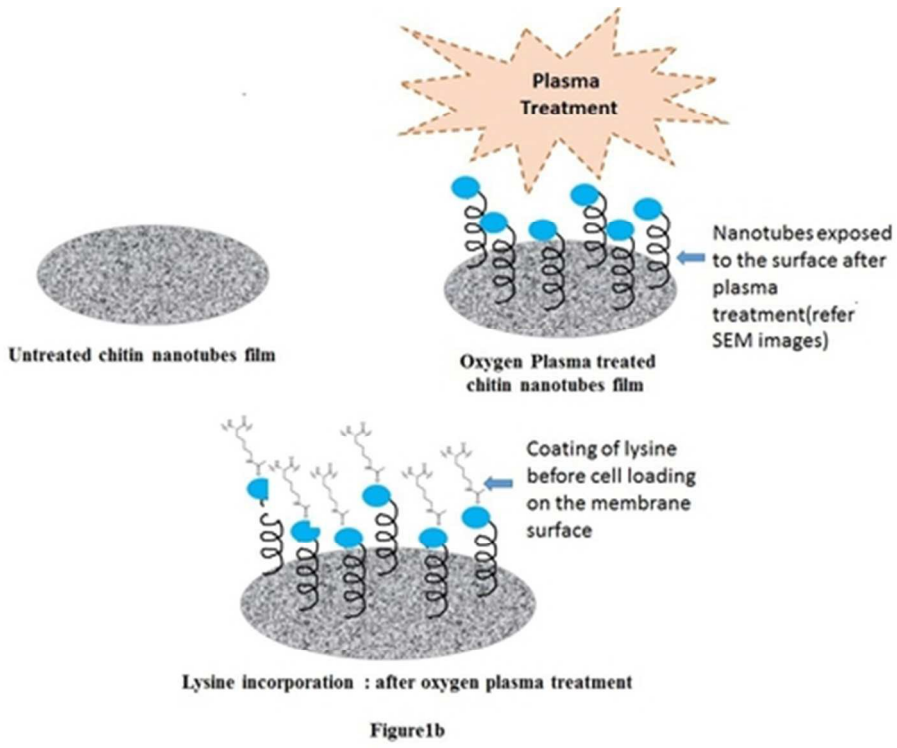

Figure1b. Schematic representation of plasma treatment of chitin/CNTs composite films.
39x36mm (300 x 300 DPI)

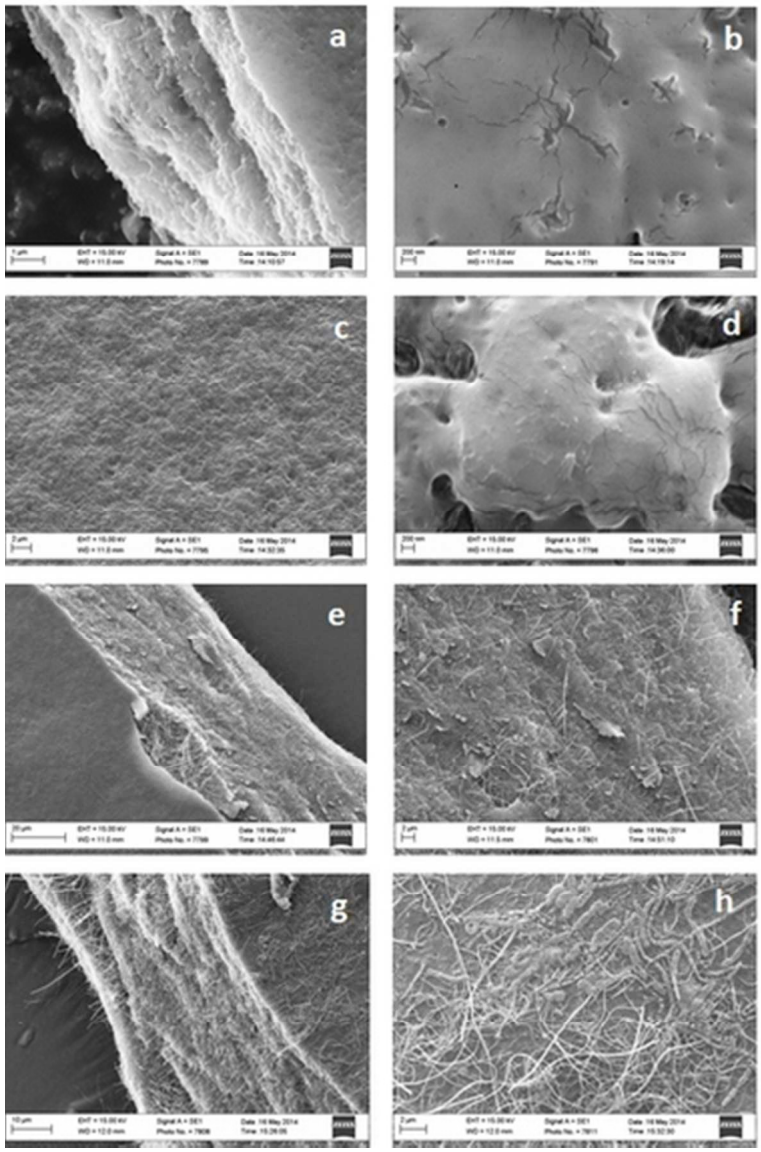

Figure 2. Scanning electron microscopy images at low (left) and high (right) resolution of chitin/CNTs composite films: a/b Chitin untreated; c/d Chitin treated; e/f Chitin/CNTs untreated; g/h Chitin/CNTs treated
32x48mm (300 x 300 DPI)

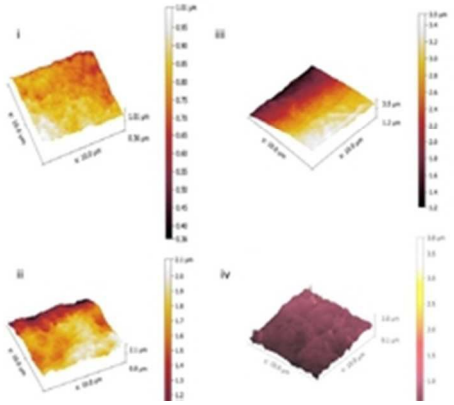

Figure 3a: Topography and surface roughness of composites from AFM imaging under ambient conditions: (i) Chitin untreated; (ii) Chitin treated; (iii) chitin/CNTs untreated; (iv) chitin/CNTs treated
30x17mm (300 x 300 DPI)

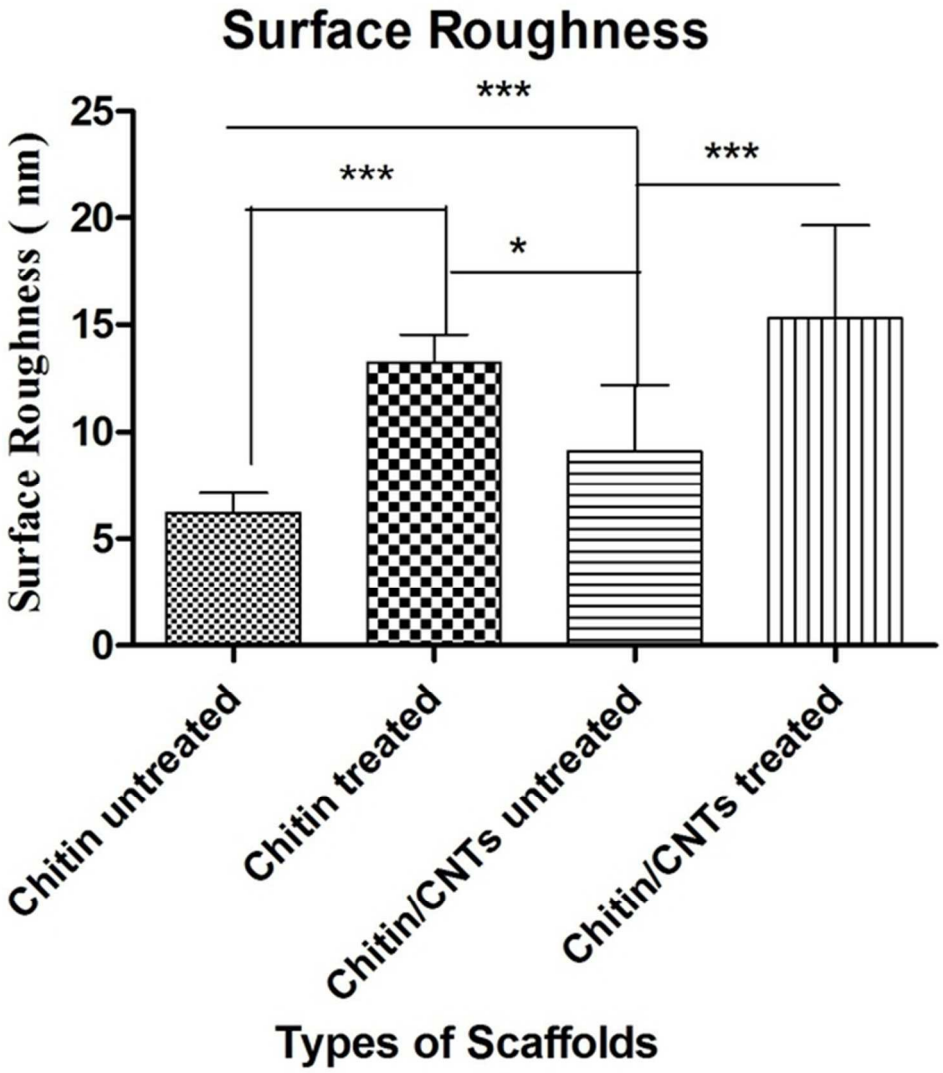

Figure 3b: Surface roughness of the four types of scaffolds showing increased surface roughness after plasma treatment. One-way ANOVA with Turkey's multiple comparison post-hoc test and a significance level of 0.05.A mean +/- standard deviation format has been used to present the data.
54x62mm (300 x 300 DPI)

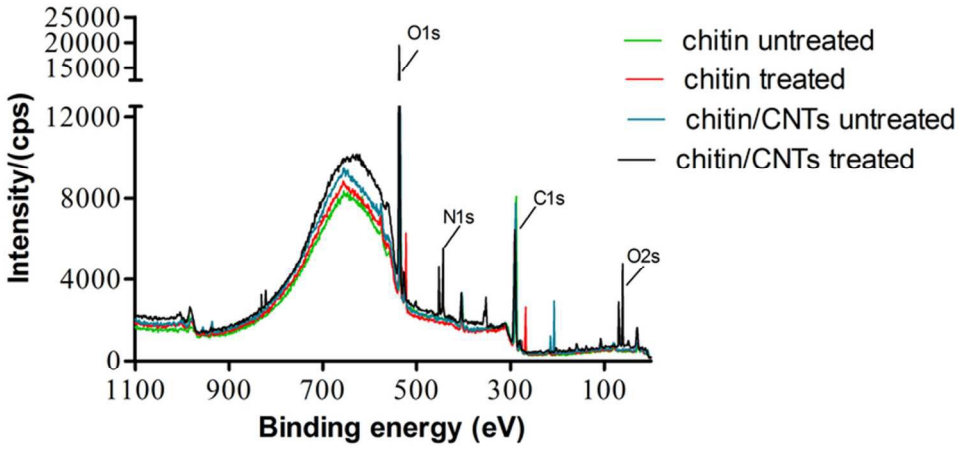

Figure 4: Comparative XPS spectra of all four scaffolds with and without O2 plasma modification.
74x37mm (300 x 300 DPI)

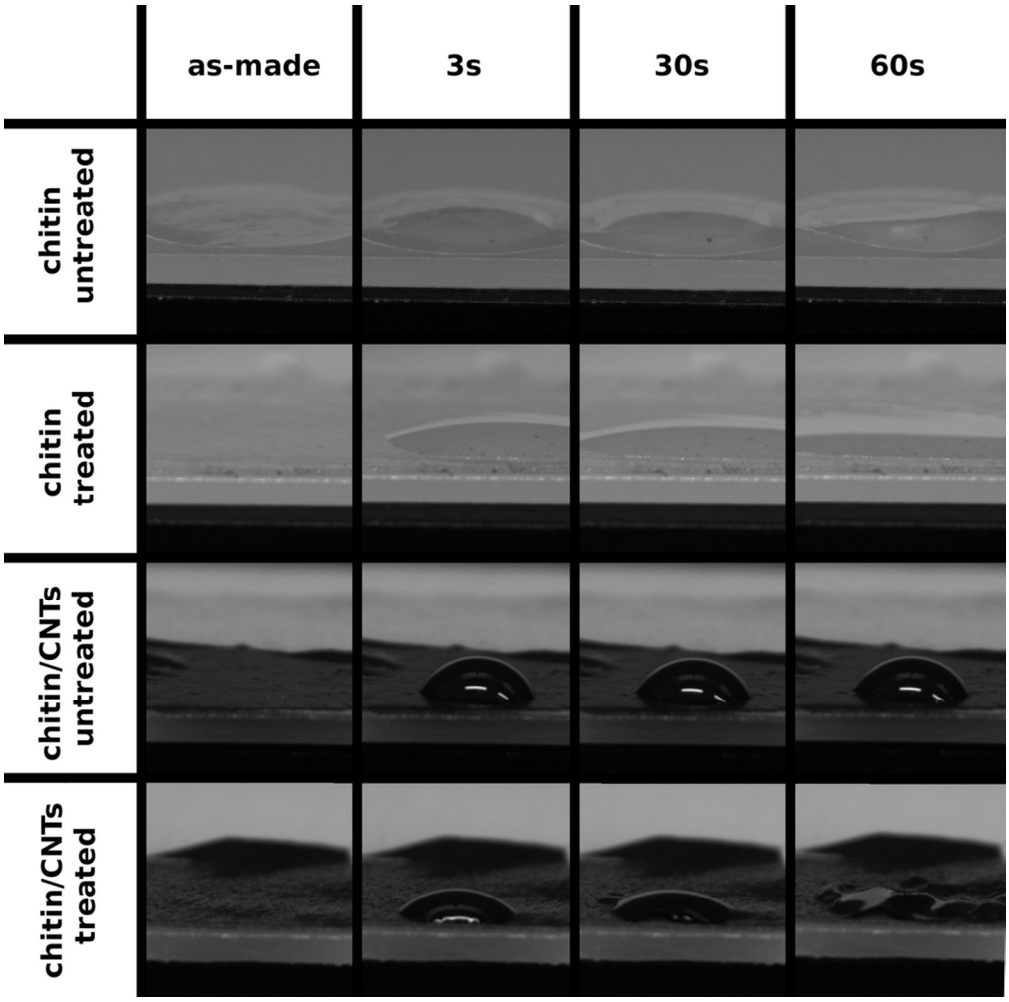

Figure 5a. The influence of plasma treatment on the water affinity of the surface of four types of scaffolds. Water droplet spreading is shown after 3s, 30s and 60s after the droplet has been placed onto the surface. Neat samples are also shown as reference.
90x89mm (300 x 300 DPI)

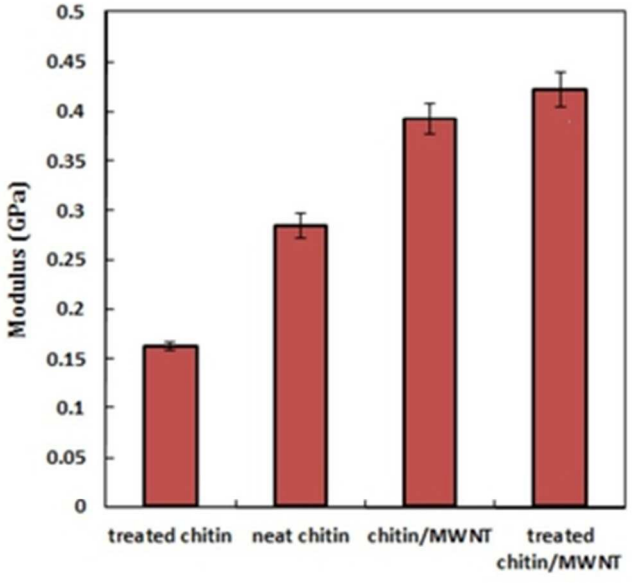

Figure 5b. Elastic modulus of the four scaffolds measured using Nano indentation.
30x26mm (300 x 300 DPI)

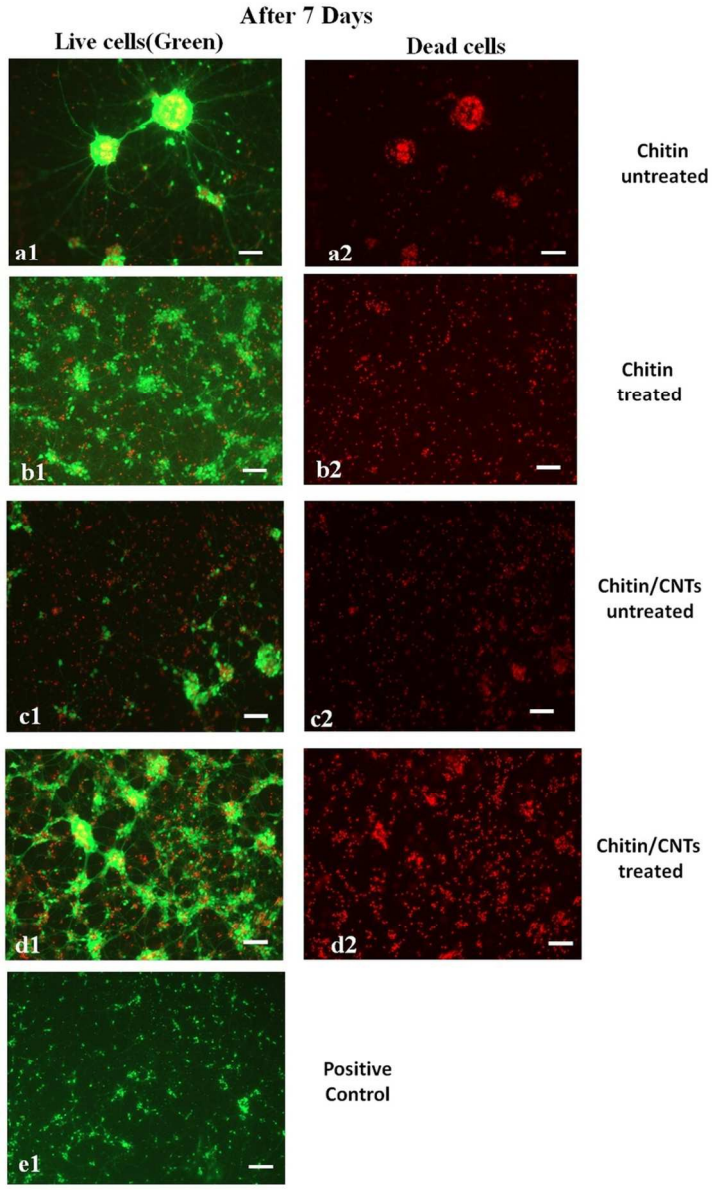

Figure 6.1. The images were obtained after 7 d of cell seeding. Scale bar represents 100um.

Live and dead assay to test the viability of cortical neurons on all the four scaffolds. Cells were seeded on the scaffolds and stained with the Live/Dead viability stain. Green cells showed the number of live cells with blue nucleus and red cells showed dead cells due to excitation of florescent dye ethidium homodimer-1, emission 568 nm.

76x127mm (300 x 300 DPI)

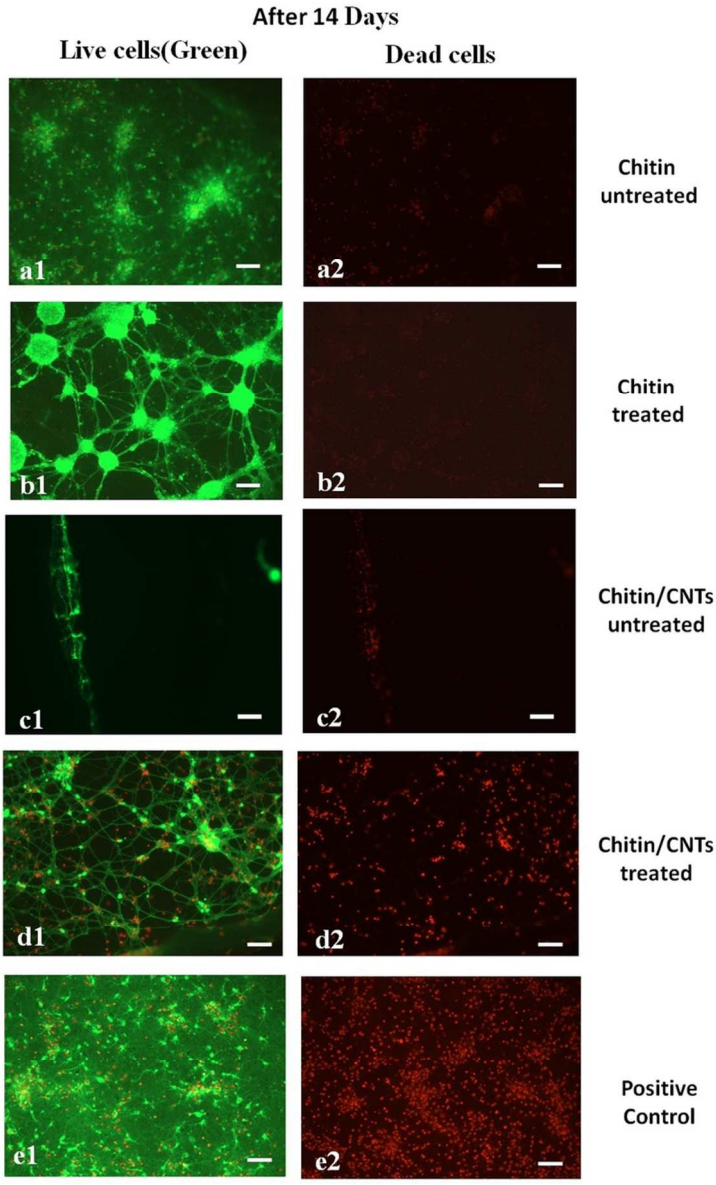

Figure 6.2. The images were obtained after 14 d of cell seeding. Scale bar represents 100 μm.

Live and dead assay to test the viability of cortical neurons on all the four scaffolds. Cells were seeded on the scaffolds and stained with the Live/Dead viability stain. Green cells showed the number of live cells with blue nucleus and red cells showed dead cells due to excitation of florescent dye ethidium homodimer-1, emission 568 nm.
68x112mm (300 x 300 DPI)

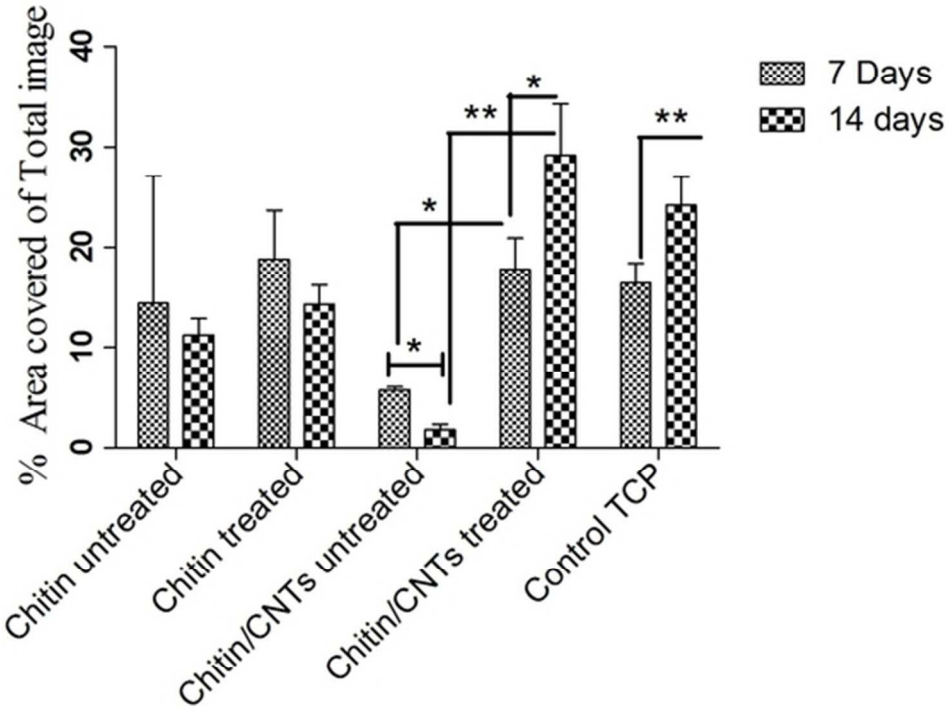

Figure 7: Percentage cell adhesion on four types of scaffolds obtained by Image J analysis of the fluorescent images obtained from the live and dead assay. For each membrane four images were analysed. The numbers of pixels were kept constant for all images. The fluorescent signal obtained for each image was converted to percentage area covered. The positive control is tissue culture plastic plate.
49x39mm (300 x 300 DPI)

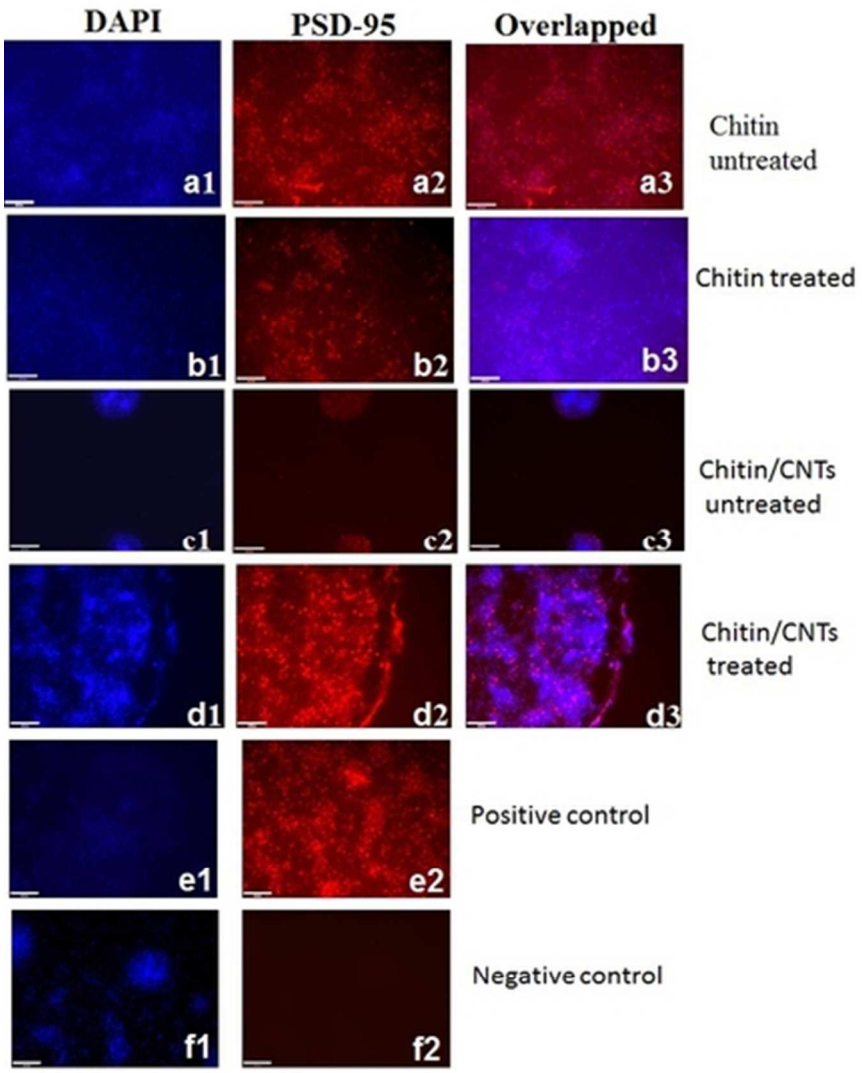

Figure 8. PSD-95 staining of all four composites after 21 d. Cells seeded on the scaffolds were stained with anti-PSD-95 antibody and counter-stained with DAPI: Chitin untreated (a1-DAPI/a2-PSD-95/a3 merged); Chitin treated (b1-DAPI/b2-PSD-95/b3 merged); Chitin/CNTs untreated (c1-DAPI/c2-PSD-95/c3 merged). Chitin/CNTs treated (d1-DAPI/d2-PSD-95/d3 merged). The positive control was tissue culture plastic plate with (e1-DAPI/e2-PSD-95). The negative control was cell growth in tissue culture wells where no primary antibody was added (f1-DAPI/f2-Negative control). Scale bar represents 120 μm.
39x46mm (300 x 300 DPI)

%	Chitin untreated	Chitin treated	Chitin /CNTs untreated	Chitin/CNTS treated
C1s	67.8	67.8	63.9	53.9
N1s	9.7	7.8	9.1	5.6
O1s	22.5	29	27	40.5
C-C	43.5	36.9	38.3	19
C-O	40.9	46.1	46.7	62.1
C=O	15.6	17	15	18.9
C(ox):C(unox)	1.3	1.7	1.6	4.3

Table1: Surface atomic composition (atomic %) of various composites tested along with O2 plasma-treated ones